Since January 2020 Elsevier has created a COVID-19 resource centre with free information in English and Mandarin on the novel coronavirus COVID-19. The COVID-19 resource centre is hosted on Elsevier Connect, the company's public news and information website.

Sensors & Actuators: B. Chemical 390 (2023) 133960

Contents lists available at ScienceDirect

Sensors and Actuators: B. Chemical

journal homepage: www.elsevier.com/locate/snb

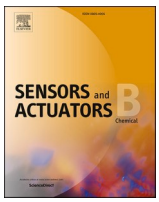

One-step-one-pot hydrothermally derived metal-organic-framework-nanohybrids for integrated point-of-care diagnostics of SARS-CoV-2 viral antigen/pseudovirus utilizing electrochemical biosensor chip

Sathyadevi Palanisamy [a,1], Li-Yun Lee [b,1], Chih-Fei Kao [b], Wen-Liang Chen [b], Hsiang-Ching Wang [c], San-Tai Shen [d], Jhih-Wei Jian [d], Shyng-Shiou F. Yuan [e,f,g], Yu-An Kung [h], Yun-Ming Wang [b,*]

[a] Institute of Biomedical Engineering, National Tsing Hua University, Hsinchu 300, Taiwan
[b] Department of Biological Science and Technology, Institute of Molecular Medicine and Bioengineering, Center for Intelligent Drug Systems and Smart Bio-devices (IDS2B), National Yang Ming Chiao Tung University, 75 Bo-Ai Street, Hsinchu 300, Taiwan
[c] Biomedical Technology and Device Research Lab, Industrial Technology Research Institute, Hsinchu 300, Taiwan
[d] AnTaimmu BioMed Co., Ltd, Unit 304, No. 1, Lixing 1st Road, East District, Hsinchu 300, Taiwan
[e] Translational Research Center, Kaohsiung Medical University Hospital, Kaohsiung Medical University, Kaohsiung 807, Taiwan
[f] Department of Obstetrics and Gynecology, Kaohsiung Medical University Hospital, Kaohsiung Medical University, Kaohsiung 807, Taiwan
[g] Faculty and College of Medicine, Kaohsiung Medical University, Kaohsiung 807, Taiwan
[h] Research Center for Emerging Viral Infections, College of Medicine, Chang Gung University, Taoyuan City, Taiwan

ARTICLE INFO

Keywords:
MOF
Sensing
Electrochemical
Chip
Device

ABSTRACT

The COVID-19 pandemic has become a global catastrophe, affecting the health and economy of the human community. It is required to mitigate the impact of pandemics by developing rapid molecular diagnostics for SARS-CoV-2 virus detection. In this context, developing a rapid point-of-care (POC) diagnostic test is a holistic approach to the prevention of COVID-19. In this context, this study aims at presenting a real-time, biosensor chip for improved molecular diagnostics including recombinant SARS-CoV-2 spike glycoprotein and SARS-CoV-2 pseudovirus detection based on one-step-one-pot hydrothermally derived $CoFeBDCNH_2$-$CoFe_2O_4$ MOF-nanohybrids. This study was tested on a PalmSens-EmStat Go POC device, showing a limit of detection (LOD) for recombinant SARS-CoV-2 spike glycoprotein of 6.68 fg/mL and 6.20 fg/mL in buffer and 10% serum-containing media, respectively. To validate virus detection in the POC platform, an electrochemical instrument (CHI6116E) was used to perform dose dependent studies under similar experimental conditions to the handheld device. The results obtained from these studies were comparable indicating the capability and high detection electrochemical performance of MOF nanocomposite derived from one-step-one-pot hydrothermal synthesis for SARS-CoV-2 detection for the first time. Further, the performance of the sensor was tested in the presence of Omicron BA.2 and wild-type D614G pseudoviruses.

1. Introduction

According to recent data, SARS-CoV-2 has reached over 458 million cumulative reported cases including 5.7 million deaths globally since March 2022 [1]. This pandemic outbreak caused by SARS-CoV-2 has become a huge burden on public life and health care professionals worldwide [2]. Ever-increasing transmission rate has become a great challenge to control [3]. Although several vaccines and antivirals specific to SARS-CoV-2 were under emergency use authorization (EUA) from the Food and Drug Administration, the development of reachable rapid diagnostic technologies is useful to control and monitor the COVID-19 pandemic [4–6]. This emergency actuates the researchers to

* Corresponding author.
E-mail address: ymwang@nycu.edu.tw (Y.-M. Wang).
[1] These two authors contributed equally.

https://doi.org/10.1016/j.snb.2023.133960
Received 26 December 2022; Received in revised form 24 April 2023; Accepted 9 May 2023
Available online 10 May 2023

develop a more efficient, marketable, and rapid POC diagnostic device to detect the causative SARS-CoV-2 virus.

The Reverse Transcriptase Polymerase Chain Reaction (RT-PCR) is being currently used as a standard methodology to detect COVID-19 but it can target the viral genome only in the nasopharyngeal or nasal samples [7]. Different proposed testing methods such as nucleic acid testing and computed tomography (CT) imaging lack rapid detection, and ease of handling to be used in a POC condition [8]. Provided the listed demerits of the available approaches and the demand for easy and early detection, a portable, real-time, ultra-sensitive alternating technology is introduced in this study for early detection of SARS-CoV-2.

The most frequently used biosensors for virus detection are mainly based on electrochemical devices [9]. The advancement in electronic designs and interlinked circuits for readout systems enable an inexpensive biosensor fabrication process [10]. The partnership of bioelectronics and technology can lead to the generation of nanoscale devices that can compete with conventional systems [11].

Metal-organic frameworks (MOFs) are a unique class of materials that are porous, crystalline, self-assembled by single or multi metal ions or metallic clusters, and organic linkers through coordination bonds [12–14]. Some studies emphasize the fitness of MOFs in integrated analytical devices [15–17]. However, MOFs alone are considered electrically insulating because of their poor-electron transfer property, which retards the straight use of MOFs in electrochemical sensing [18, 19]. To address this demerit, MOF-composites platforms were introduced in which the MOFs can be incorporated with conducting materials to enhance electron transfer ability and act as electrochemical sensors [20,21]. So far generated MOF-nanohybrids involves tedious, time-consuming, multi-step synthetic methods and characterization. Hence, in this study, a new attempt was made to minimalize the synthesis efforts and successfully achieved $CoFeBDCNH_2$-$CoFe_2O_4$ MOF-nanohybrids preparation in a one-step-one-pot hydrothermal reaction. The integration of high surface area MOFs and high electron conductivity of nanomaterials enables the MOF-nanohybrids an excellent sensor [22]. Thus, it is expected that the synergistic effects of MOF and $CoFe_2O_4$ in the MOF-nanohybrids would effectively enhance the electrode efficiency and stabilize the hybrids to undergo electrochemical reactions. Furthermore, the synergies of MOFs and $CoFe_2O_4$ in MOF-nanohybrids were evaluated towards SARS-CoV-2 spike protein detection electrochemically, including the recombinant viral glycoprotein and the pseudovirus.

In this study, a commercial PalmSens-EmStat GO system was chosen as it facilitates the application of various electrochemical measurements including EIS without requiring extensive knowledge regarding firmware and digital electronics. Additionally, the miniaturized module (Production of electrodes, Scheme S1) allows for affordable, portable, and rapid electrochemical detection, which is suitable for point-of-care use. It is portable, cheap, and enables rapid sensor prototyping but it requires basic programming knowledge that can be considered a major hindrance in this study. Herein, this work presents a real-time, biosensor test strip for improved molecular diagnostics using a one-step-one-pot hydrothermally synthesized $CoFeBDCNH_2$-$CoFe_2O_4$ MOF-nanohybrids-modified gold chip as the substrate. The gold chip electrode modified with such MOF-nanohybrids provides a high surface area which is further applied to increase the target binding on the electrode surface. Furthermore, the SARS-CoV-2 specific antibodies were conjugated onto the electrode surface in an ordered orientation through a self-assembled monolayer (SAM) using 11-Mecaptoundecanoic acid (11-MUA) as a linker. Accordingly, the sensitivity of the fabricated electrode significantly increased the direction of the SARS-CoV-2 viral antigen. These test strips allows the possibility of on-site screening using a low volume of testing samples. In addition, it is further compared against a commercial instrument "CHI 6116E CH Electrochemical Analyzer" to compare the electrochemical performances in buffer and serum-containing media.

2. Materials and methods

The details of the experimental methods are provided in the supporting information.

3. Results and discussion

3.1. Design and sensing strategy of MOF-nanohybrid platform

In this report, we developed a simple one-step-one-pot hydrothermal, various Fe-MOFs, and nanomaterial-evolved process to produce hollow porous $CoFe_2O_4$ combined $CoFeBDCNH_2$ MOF-nanohybrid as the material for POC diagnostics (Scheme 1). To the best of our knowledge, this is the first report utilizing the one-step-one-pot hydrothermal derived MOF-nanohybrids for the SARS-CoV-2 viral antigen sensing. The integration of high surface area MOFs and high electron conductivity of nanomaterials enables the MOF-nanohybrids an excellent sensors [22]. Such a super combo can surpass the performance of original elements [22,23]. Thus, it is expected that the synergistic effects of MOF and $CoFe_2O_4$ in the MOF-nanohybrids would effectively enhance the electrode efficiency and stabilize the hybrids to undergo electrochemical reactions.

Additionally, the electrochemical activity is investigated individually for each material isolated at different reaction times so that the conductive effect of each material can be determined to ultimately identify the most suitable material to work towards the SARS-CoV-2 viral antigen detection. Therefore, the sensing competence of the newly fabricated electrodes was explored using electrochemical impedance spectroscopic (EIS) measurements. Finally, the MOF-nanohybrids formed at a reaction time of 120 min were used as the substrate for the SARS-CoV-2 viral antigen detection as they displayed the best conductivity among all the products obtained.

3.2. Evolution of the $CoFeBDCNH_2$-$CoFe_2O_4$ MOF-nanohybrids and their structural investigations

The surface topology of the materials obtained from the hydrothermal reactions at increasing reaction times 30 min, 60 min, 90 min, 120 min, 10 h, and 24 h analyzed using scanning electron microscopy (SEM) is summarized in Fig. S1.

The reaction path for the evolution of MOF composite from the hydrothermal reactions can be analyzed from the surface topology results. The results estimate the structural morphology and the conversion of the product composition are shown in Fig. S1. It is noted that in the initial stage of the reaction times, at 30 min, a mixture of comparable portions of the two different have appeared. When the reaction time is further increased to 60 min and 90 min, both the MOFs remain to be the same mixture. Among them, one product was identified with spindle morphology and the other product as particulate type. The spindle shaped products here were assigned as MIL-88B(Fe)-NH_2 and the other particulate type is meant to be MIL-53. The absence of cobalt ions in the elemental composition obtained from Energy-Dispersive-X-ray Analysis (EDX) clearly shows the formation of iron based MOFs alone until 90 mins (Fig. S1). When the reaction proceeded further up to 120 mins, the mixture of MIL-53 and MIL-88B(Fe)-NH_2 disappeared and the formation of MOF-nanohybrids appeared with chunk morphology. The hybrid material obtained is the combination of $CoFeBDCNH_2$ MOFs and a spinel ferrite $CoFe_2O_4$. The SEM-EDX elemental composition is evident in the presence of both cobalt and iron (Fig. S2). When the reaction time is exceeded over 120 min, a mixture of two different products $CoFe_2O_4$ and $CoFeBDCNH_2$ MOFs were identified at 10 h, with $CoFe_2O_4$ as a dominant one. The SEM-EDX data and mapping analysis further support the increasing $CoFe_2O_4$ formation (Fig. S2). At the reaction time of 24 h, the spindle-shaped products completely disappeared and only particulate materials remains. The only material that remains after 24 h reaction time was found to be $CoFe_2O_4$. The SEM-EDX elemental data

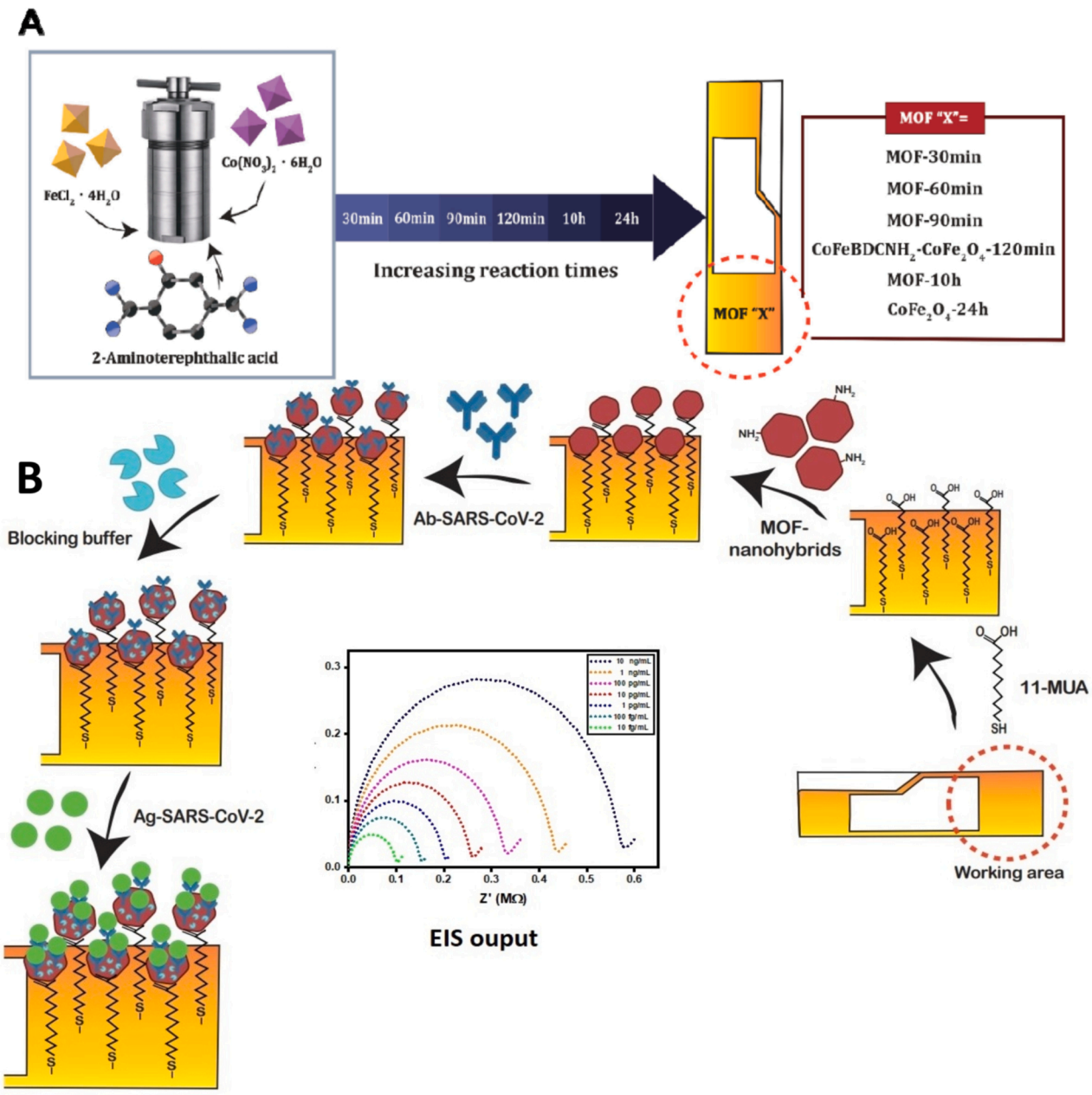

Scheme 1. (A) Schematic illustration for the time dependent one-step-one-pot hydrothermal synthesis of $CoFeBDCNH_2$-$CoFe_2O_4$ MOF-nanohybrids and other products at increasing reaction times. (B) Schematic representation of fabrication and sensing strategy of MOF-nanohybrids platform for the SARS-CoV-2 viral antigen detection using a handheld, portable device.

indicates the complete formation of $CoFe_2O_4$ (Fig. S2). It is widely accepted that the electrochemical performances are highly dependent on the morphology of the electrode materials including the size and shape [24–28]. Also, it is identified that the materials with hierarchial and porous architectures can exhibit excellent electrochemical behavior owing to the presence of effective surface properties, structural stabilities, and shorter diffusion paths of electrolytic ions due to the close contact between the electrode and electrolyte [29,30]. In this study, the obtained porous MOF-nanohybrids with hierarchially oriented nanosheets-like morphology are expected to have potential electrochemical properties when analyzing biosensing applications. The complete transitions in the evolution of the MOF-nanohybrids were further studied by XRD studies. Several other studies were performed to confirm the final product as well.

As the sensor performance is particularly reliant on the microstructure of the sensing element, it is important to investigate the morphology of the obtained nanomaterials. The formation of $CoFeBDCNH_2$-$CoFe_2O_4$ MOF-nanohybrids and pure $CoFe_2O_4$ at reaction times 120 min and 24 h, respectively, were characterized by TEM analysis (Fig. 1) which not only throws light on morphological structures but also on the size of the products. The MOF-nanohybrids along with the longer reaction time product $CoFe_2O_4$ were characterized for comparison (Fig. 1). The high and low magnification TEM images are shown in Fig. 1, indicating that the MOF-nanohybrids are composed of crystalline nanosheets-like morphology $CoFeBDCNH_2$ and spherical $CoFe_2O_4$ with the size of 200 nm. The HR-TEM images of the final product with the interfinge distance of 0.26 nm are shown in Fig. S3. The elemental composition of the as-synthesized MOF-nanohybrids and pure $CoFe_2O_4$ were further analyzed with TEM-EDX and elemental mapping analysis (Fig. 1). Additional TEM images, TEM-EDX spectra, and the elemental mapping recorded for the final 24 h product, $CoFe_2O_4$ can be found in Fig. S4.

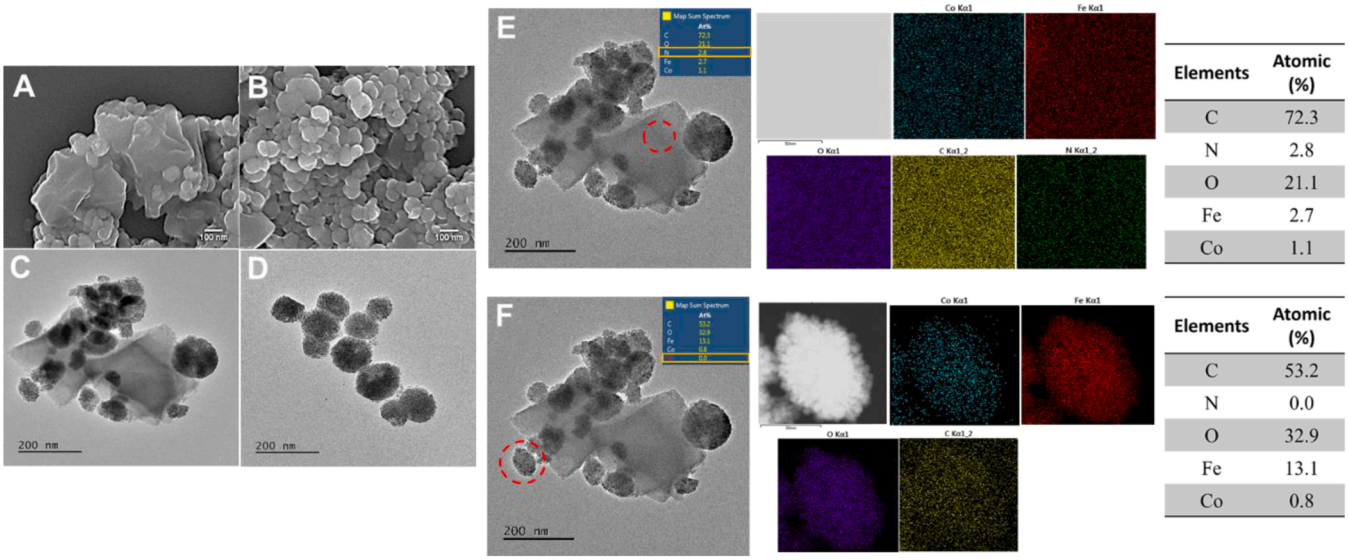

Fig. 1. (A-D) SEM images of $CoFeBDCNH_2$-$CoFe_2O_4$ MOF-nanohybrids obtained from the hydrothermal reaction at 120 min (100 nm scale bar). (E) TEM-EDX elemental mapping images of $CoFeBDCNH_2$-$CoFe_2O_4$ MOF-nanohybrids highlighting the formation of $CoFeBDCNH_2$ obtained from the hydrothermal reaction at 120 min (200 nm scale bar). (F) TEM-EDX elemental mapping images of $CoFeBDCNH_2$-$CoFe_2O_4$ MOF-nanohybrids highlighting the formation of $CoFe_2O_4$ obtained from the hydrothermal reaction at 120 min.

Despite the availability of various synthetic approaches to limit the growth of MOF nanoparticles and nucleation, the formation of mixed-phase MOFs obtained from one-pot solvothermal synthesis is inevitable [31–33]. The formation of MOFs with different secondary building units leads the metal clusters to attain uncertain surface areas, indistinct pore structures, etc., which remarkably limit their applications [34,35]. It is reported that the MIL-88(Fe) MOF can be transformed to 3D Fe_3O_4/C with controlled particle size and shape and is further used for electrochemical studies [36]. Therefore, in this study, the formation of a mixture of two particle populations MIL-88B(Fe)-NH_2/MIL-53 and $CoFeBDCNH_2$-$CoFe_2O_4$ MOF-nanohybrids from the one-step-one-pot hydrothermal synthesis in the initial stage of the reactions is reasonable [37].

Additionally, the XRD patterns were recorded to evaluate the product formations at different reaction times. The analysis was performed to understand the phase composition and to ensure that all the synthesized products were free of impurities. The phase structures of all the hydrothermal products are shown in Fig. S5. The XPS survey was recorded to gain knowledge of the chemical and electronic states of the synthesized materials. The recorded survey clearly illustrated the presence of elemental components (Co, Fe, C, N, and O) in the MOF-nanohybrids (Fig. S6). The Co_{2p} XPS spectrum of MOF-nanohybrids displayed two major peaks at 779.7 eV and 795 eV are attributed to the presence of $Co2p_{3/2}$ and $Co2p_{1/2}$, respectively. This indicates that the cobalt ion present in the MOF-nanohybrids is in the + 2-oxidation state. This identification is further verified by the formation of two satellite peaks at 803 eV and 787 eV corresponding to the Co^{2+}. The two other major peaks displayed at 710.6 eV and 723 eV reveal the presence of $Fe2p_{3/2}$ and $Fe2p_{1/2}$, respectively. The Fe in the $CoFeBDCNH_2$-$CoFe_2O_4$ acquired a + 3 oxidation state which is further verified by the presence of two satellite peaks at 717 eV and 731 eV related to iron. The C1s peaks located at 284 eV are assigned for C-C groups and the N1s peaks found at 399 eV are related to C-N formation. Overall, the XPS survey determines the formation of $CoFeBDCNH_2$-$CoFe_2O_4$ hybrids. The FT-IR recorded for $CoFeBDCNH_2$-$CoFe_2O_4$ MOF-nanohybrids was obtained from the hydrothermal reaction at 120 min (Fig. S7).

3.3. Stepwise fabrication of $CoFeBDCNH_2$-$CoFe_2O_4$ MOF-nanohybrid modified gold electrodes

Fig. S8 depicts the pictorial representation of the device and its setup used for electrochemical measurements. Competitive EIS measurements of MOF'X' products isolated from different reaction times are given in Fig. S9. Before this analysis, the stability of Ab-SARS-CoV-2 was tested by dot blot assay. The resulting dot formation confirms the stability of the antibody as shown in Fig. S10.

Fig. 2 demonstrates the impedance spectra for the redox probe recorded during stepwise electrode fabrication processes of the gold chip simulated using Randle's equivalent circuit (Fig. S11). In the first step, the EIS spectra were recorded for the bare gold chip and noted their R_{ct}. Then, the EIS spectra of the SAM of the carboxylic-terminated group on the gold surface show the typical impedance semi-circles which represent the electron transfer. On the other hand, a decrease in the charge transfer was noticed after the decoration of MOF-nanohybrids on the gold surface, indicating the MOF-nanohybrids catalyze the charge-

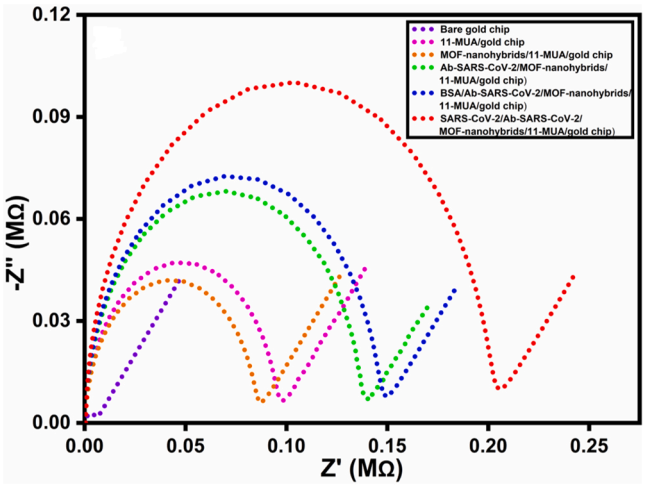

Fig. 2. EIS measurements during the fabrication process of $CoFeBDCNH_2$-$CoFe_2O_4$ MOF-nanohybrid modified gold electrodes in the presence of [1:1] redox probe, pH 7.4 in a buffered media.

transfer process of $[Fe(CN)_6]^{3-/4-}$. After immobilizing the Ab-SARS-CoV-2 on the $CoFeBDCNH_2$-$CoFe_2O_4$/11-MUA/gold chip electrode, the semicircle diameter increased due to high resistance and decreased electron transfer. Then, the non-specific binding sites were blocked using the bovine serum albumin (BSA), and set the electrodes for binding with SARS-CoV-2 spike protein. Finally, the EIS was recorded for the electrodes after binding with the SARS-CoV-2 spike protein of concentration 1 pg/mL. The R_{ct} is found to be highly increased probably due to the steric hindrance and blocking of the electron transfer by antibody-antigen binding. It is found that the MOF-nanohybrid modified electrode is very reliable and sensitive sufficient for the SARS-CoV-2 viral antigen detection, demonstrating the synergistic effects of MOFs and porous $CoFe_2O_4$ in the MOF-nanohybrids. The amount of antibody bound on the electrodes was further quantified by the enzyme-linked immunosorbent assay (ELISA) (Fig. S12, Table S1). All the MOF'X' electrodes used in the competitive EIS measurements were also prepared using the same method. Additionally, the EIS recorded for a batch of electrodes during each step of electrode fabrication is given in Figs. S13–S17.

3.4. Surface topography analysis by SEM during the fabrication of $CoFeBDCNH_2$-$CoFe_2O_4$ MOF-nanohybrid sensor

To further investigate the antibody conjugation on $CoFeBDCNH_2$-$CoFe_2O_4$/11-MUA/gold chip composite electrodes, SEM analyses were performed. During the fabrication of each step of the electrode construction, the morphological changes were recorded and the results are displayed in Fig. S18. The result illustrates the SEM images obtained after the electrode material, MOF-nanohybrid was introduced on the 11-MUA linked gold chip electrode. The electrode surface became rough after the attachment of $CoFeBDCNH_2$-$CoFe_2O_4$ on the electrodes as shown in Fig. S18A. The immobilization of antibodies on the $CoFeBDCNH_2$-$CoFe_2O_4$/11-MUA/gold chip electrode yields visible globular structures suitable for the SARS-CoV-2 viral antigen binding. The recorded SEM images of antibody conjugated electrodes are shown in Fig. S18B. The treatment of the SARS-CoV-2 spike protein (1 ng/mL) on the Ab-SARS-CoV-2/$CoFeBDCNH_2$-$CoFe_2O_4$/11-MUA/gold chip electrode shows decreased globular structures, suggesting the antibody-antigen interactions (Fig. S18C) [38]. Clear, morphological changes on the surface modified electrodes are evidence of the successful fabrication of the electrodes and the SARS-CoV-2 spike protein detection.

3.5. Analytical ability of $CoFeBDCNH_2$-$CoFe_2O_4$ MOF-nanohybrid platform towards SARS-CoV-2 detection

To demonstrate the detection range in patient samples, presently Taiwan has imposed high restrictions on using real COVID samples for research purposes. At the same time, it is important to validate the performance of the sensor using high standard methods. Therefore, this study makes use of a pseudovirus system for the application as an alternative approach to mimic a real scenario. Pseudovirus systems can effectively screen vaccines outside of a biosafety level BSL-3 or BSL-4

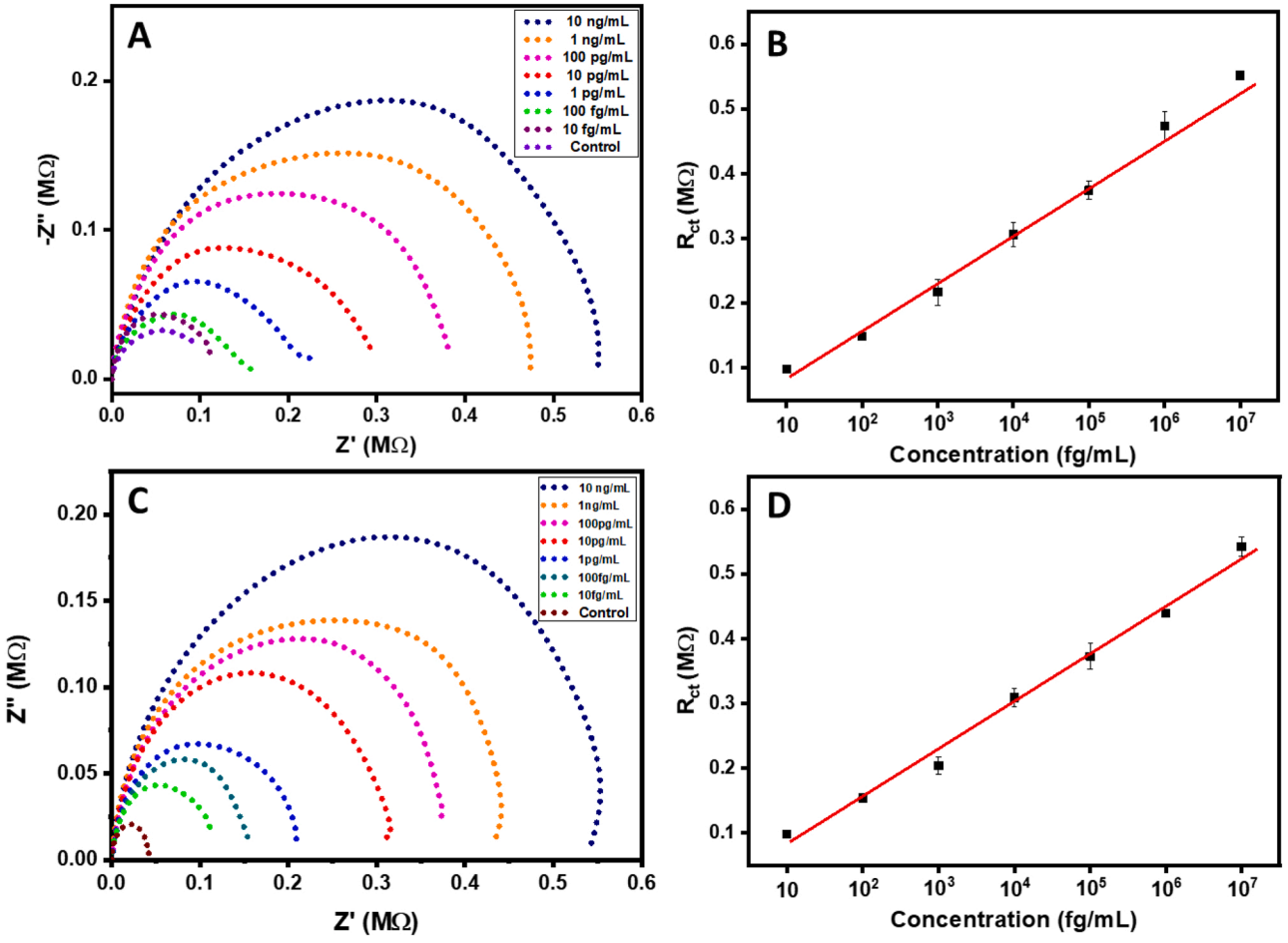

Fig. 3. (A) Nyquist plots obtained after the treatment of various concentrations of SARS-CoV-2 viral antigen ranging from 10 ng/mL to 10 fg/mL in the presence of [1:1] redox probe, at a pH 7.4 under buffer media. (B) A linear plot was obtained from R_{ct} [MΩ] versus SARS-CoV-2 concentration for (A). (C) Nyquist plots were obtained after the treatment of various concentrations of SARS-CoV-2 antigen ranging from 10 ng/mL to 10 fg/mL in the presence of [1:1] redox probe, at pH 7.4 in 10% serum-containing solution. (D) A linear plot was obtained from R_{ct} [MΩ] versus SARS-CoV-2 concentration for (C).

level laboratory conditions. Utilizing this method allows them to be safely handled in BSL-2 laboratories and can avoid the handling of highly infectious viruses. The numerous benefits associated with pseudoviruses triggered us to perform scientific research on the detection of SARS-CoV-2 viral antigen. This is the real reason why this work employed pseudo virus investigations in our study instead of real COVID samples [39,40].

The fabricated sensors were tested for various concentrations of the SARS-CoV-2 spike protein ranging from 10 ng/mL to 100 fg/mL in buffer and 10% serum media. The Nyquist plots recorded for the EIS measurements are shown in Figs. 3 and 4. It shows the sequential impedance changes obtained after the SARS-CoV-2 spike protein binding on the Ab-SARS-CoV-2 modified electrode. The R_{ct} is chosen as the parameter to quantify the immunosensor response. It is found from the EIS measurements that increasing the spike protein concentrations increases the charge transfer resistance. This indicates the increasing charge transfer resistance for the redox probe and confirms the increased steric hindrance and the antibody-antigen interactions. The diameter of the respective semicircle was observed to increase following the SARS-CoV-2 spike protein concentration parallel to charge transfer resistance. The charge transfers of the $[Fe(CN)_6]^{3-/4-}$ were impeded by spike protein binding on the electrode surface. Here, a redox process with charge transfer kinetics as the rate-determining step brings a semicircular feature in a Nyquist plot of the imaginary impedance factor (Z_{imag}) versus the real impedance component (Z_{real}) in a given frequency range. The MOF-nanohybrids consequently provided a high surface area for the electrochemical reaction to proceed. Moreover, the electrical conductivity was reduced on the account of the restriction in the electrolyte diffusion towards the gold surface as a result of the antigen layer. An increase in the antibody-antigen binding causes a major kinetic barrier for electron transfer to take place. Additionally, it can potentially block the active sites on the working electrode. The EIS sensing data were obtained for three repetitive measurements. According to the obtained Nyquist plots (Fig. 3A and C), it is indicated that the EIS response of the MOF hybrid electrode exhibited a high R_{ct} towards the SARS-CoV-2 spike protein recognition, revealing the synergistic effects of high surface area MOF and highly conductive porous $CoFe_2O_4$ nanomaterials promotes the electron transfer and accelerates the electrochemical activity. Additionally, there may be due to the electrostatic interactions between amino units of MOF materials and negatively charged carboxylic units. It is mentioned that the clinically relevant quantification range is between 0.4 and 2500 U/mL and 0.8 U/mL is used as a cutoff for positivity [41]. This study achieved a wide linear range of detection between the concentration range of 10 ng/mL to 100 fg/mL with an assay time of < 5 min. The LOD was calculated as 6.68 fg/mL when tested in buffer media (Fig. 3B). When the proposed device is tested in 10% serum media, the dose-dependent study achieved the LOD of 7.25 fg/mL (Fig. 3D).

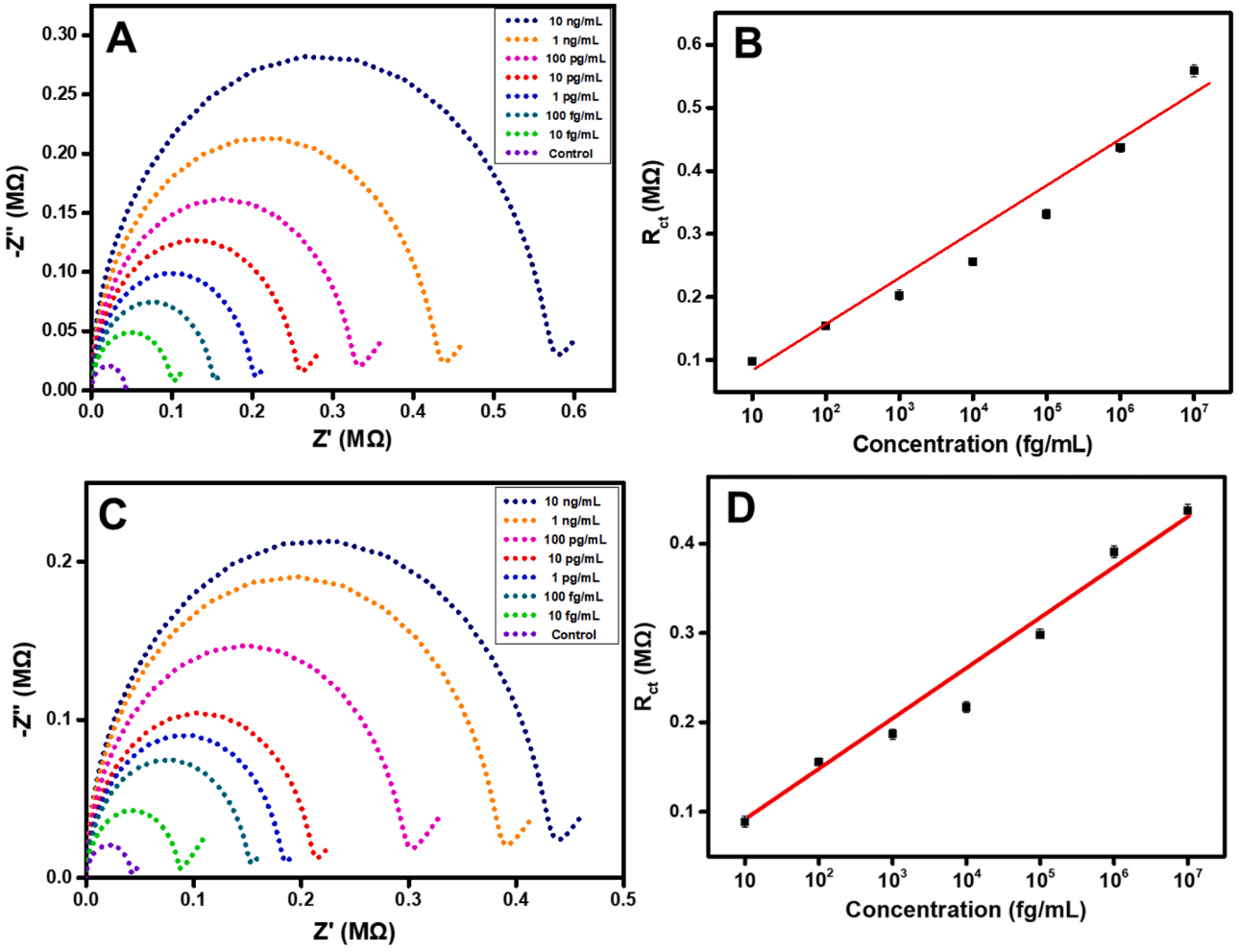

Fig. 4. (A) Nyquist plots obtained after the treatment of various concentrations of the SARS-CoV-2 viral antigen ranging from 10 ng/mL to 10 fg/mL in the presence of [1:1] redox probe, at a pH 7.4 under buffer media. (B) A linear plot was obtained from R_{ct} [MΩ] versus SARS-CoV-2 concentration for (A). (C) Nyquist plots were obtained after the treatment of various concentrations of SARS-CoV-2 antigen ranging from 10 ng/mL to 10 fg/mL in the presence of [1:1] redox probe, at pH 7.4 in 10% serum-containing solution. (D) A linear plot was obtained from R_{ct} [MΩ] versus SARS-CoV-2 concentration for (C).

3.6. Validation of the developed $CoFeBDCNH_2$-$CoFe_2O_4$ MOF-nanohybrid sensor with commercial CH instrument

The utility of the proposed biodevice was further validated for the recognition of the SARS-CoV-2 spike protein using commercial instruments. Here, the dose-dependent studies were carried out to know the status of antibody-antigen interactions in buffer (Fig. 4A) and 10% serum (Fig. 4C) media similar to that of the device. When tested in buffer solutions, the LOD of 7.35 fg/mL was obtained (Fig. 4B) whereas, in 10% serum solutions, the LOD was found to be 7.24 fg/mL (Fig. 4D) with an assay time of 10 min. The LOD obtained for the buffer and serum conditions are comparable. The obtained results validated the sensor as an effective tool for the specific spotting of the SARS-CoV-2 viral antigen both in buffer and serum samples with high accuracy.

This study compares the conductivity and electrochemical performance of the electrode with and without MOF nanohybrids to analyze the importance of the material. Further, the limit of detection and detection time was also calculated. The LOD was found to be 7.7 pg/mL (Fig. S19) and the assay time was found to be 13 min when recorded in PBS solution. A critical comparison of SARS-CoV-2 detection methods and their sensitivities with those previously reported sensors (Table S2). Detailed analysis of the reported sensor investigations decides that this material is the first ever one-step-one-pot hydrothermally derived MOF-nanohybrids used for the SARS-CoV-2 viral antigen recognition using a handheld-portable device.

3.7. Device performance towards pseudoviruses

To explore the analytical performance of the device, a set of pseudovirus samples such as Omicron BA.2 and wild-type D614G were analyzed. Here, dose-dependent studies were carried out to identify the status of antibody-antigen interactions in the buffer. It is found from the EIS measurements that increasing the pseudovirus concentrations (0 RIU, 2.7 RIU, 8 RIU, 25 RIU, 74 RIU, 222 RIU, 667 RIU, 2000 RIU, and 6000 RIU) increases the charge transfer resistance (Figs. 5 and S20), confirms the increased steric hindrance and the antibody-antigen interactions. This sensor achieved the LOD of 5.16 RIU and 9.34 RIU towards omicron BA.2 and wild-type D614G, respectively.

3.8. Selectivity, reproducibility, and stability of the designed sensor

To determine the specificity of the Ab-SARS-CoV-2/$CoFeBDCNH_2$-$CoFe_2O_4$/11-MUA/gold chip electrode for spike protein detection, the EIS experiments were conducted in which the MOF-nanohybrid modified electrode was used to assess its sensor performance. The selectivity of the nanocomposite electrode was examined by successive addition of interfering species including human enterovirus A71 (EVA71), influenza A virus, lentivirus, human coronavirus (HCoV-229E) (10,000 PFU/mL), indicating no significant interference while sensing the SARS-CoV-2 spike protein at the tested concentration (1 ng/mL) as shown in Fig. 6A.

From a commercial perspective, reproducibility and stability are the two most desired parameters to be considered. Therefore, the electrodes were produced from five different batches and one electrode from each of the batches, a total of five of the electrodes were tested for EIS in the presence of the SARS-CoV-2 spike protein concentration of 1 ng/mL. The R_{ct} values obtained from each electrode reveal that this fabrication methodology yields identical electrodes that are most suitable for the SARS-CoV-2 spike protein detection (Fig. 6B).

The experiments on MOF-nanohybrid sensor stability by EIS demonstrated that the Ab-SARS-CoV-2 surface modified gold chip electrode displayed identical R_{ct} values as that of the initial one even after 21 days. The electrodes displayed similar values when stored at 4 °C (Fig. S21) or even stored at room temperature (Fig. S22). This indicates that the electrodes can be stored for three weeks with an ignorable reduction in sensing performance, illustrating the good stability of the electrode. Additionally, the pH stability of the electrodes was tested under different pH conditions. The results displayed that the electrodes were highly stable irrespective of their pH condition as shown in Fig. S23.

4. Conclusions

In this study, we reported the development of a biosensor test strip for the SARS-CoV-2 viral antigen detection using a handheld portable POC device and further compared against a commonly used electrochemical instrument (CHI6116E). The experiments were performed on a PalmSens-EmStat Go POC device and the LOD was found to be 6.68 fg/mL and 6.20 fg/mL when tested in buffer and serum media, respectively with high accuracy and specificity. The synergistic effects of $CoFeBDCNH_2$-MOFs and $CoFe_2O_4$-nanomaterials as MOF-nanohybrids may lead to a betterment in the electrochemical detection of various targets. This design concept possesses essential flexibility for being remodeled to detect not only the SARS-CoV-2 viral antigen but also any other disease-based biomarkers by modifying the sensor surface with the target specific antibodies. We anticipated that this strategy may provide researchers to establish a newfangled MOF-nanohybrid sensing system for the immediate detection of disease-based biomarkers. Future work

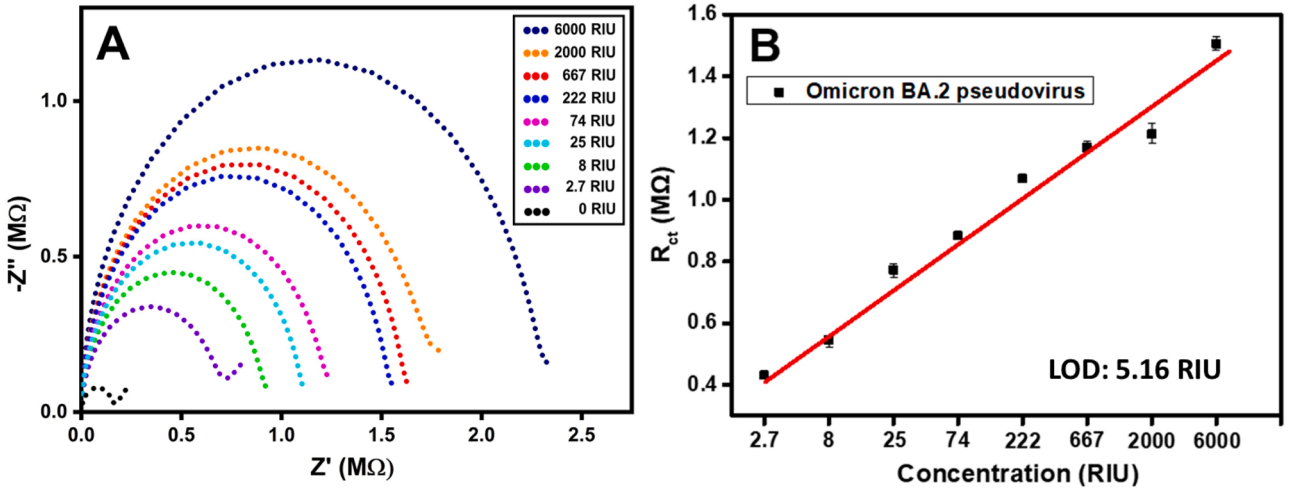

Fig. 5. (A) Nyquist plots obtained after the treatment of various concentrations of Omicron BA.2 ranging from 0 RIU to 6000 RIU in the presence of [1:1] redox probe, at a pH 7.4 under buffer media. (B) A linear plot was obtained from R_{ct} [MΩ] versus Omicron BA.2 concentration for (A).

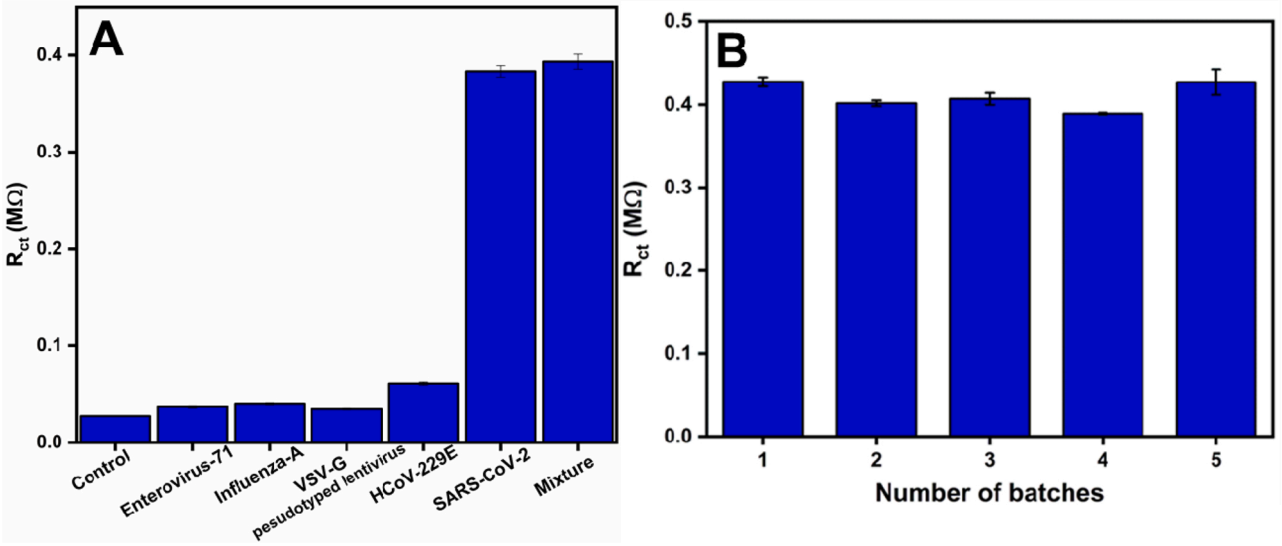

Fig. 6. (A) Selectivity of Ab-SARS-CoV-2/CoFeBDCNH$_2$-CoFe$_2$O$_4$/11-MUA/gold chip electrodes towards the SARS-CoV-2 viral antigen (1 ng/mL) detection against 1000 PFU/mL interfering species including enterovirus A71, influenza A virus, VSV-G pseudotyped lentivirus, HCoV-229E, and mixture (enterovirus A71, influenza A virus, VSV-G pseudotyped lentivirus, HCoV-229E, and Ag-SARS-CoV-2). (B) The R_{ct} measurements of MOF-nanohybrids electrodes were produced from different batches of fabrications to check their reproducibility.

concerns the deeper investigation of time-dependent and real sample analyses including human saliva or nasal swabs. The developments may focus on the translation of biosensing units from academic studies to clinical utilization for improved usability of POC detections.

CRediT authorship contribution statement

Sathyadevi Palanisamy: Conceptualization, Methodology, Validation, Formal analysis, Investigation, Writing – original draft, Writing – review & editing. **Li-Yun Lee:** Data curation, Formal analysis, Graph making. **Chih-Fei Kao:** Validation, Investigation. **Wen-Liang Chen:** Validation, Investigation. **Hsiang-Ching Wang:** Validation, Resources, Methodology, Formal analysis. **San-Tai Shen:** Validation, Investigation. **Jhih-Wei Jian:** Validation, Investigation. **Shyng-Shiou F. Yuan:** Validation, Resources. **Yu-An Kung:** Validation, Investigation. **Yun-Ming Wang:** Visualization, Supervision, Funding acquisition, Project administration.

Declaration of Competing Interest

The authors declare that they have no known competing financial interests or personal relationships that could have appeared to influence the work reported in this paper.

Data availability

Data will be made available on request.

Acknowledgments

The authors want to gratefully thank the financial supports by the National Science and Technology Council NSTC110-2113-M-A49-003, the “Center for Intelligent Drug Systems and Smart Bio-devices (IDS2B)” and “Smart Platform of Dynamic Systems Biology for Therapeutic Development” project from The Featured Areas Research Center Program within the framework of the Higher Education Sprout Project by the Ministry of Education (MOE) in Taiwan. This work was also funded by the Higher Education Sprout Project of the National Yang Ming Chiao Tung University and Ministry of Education (MOE) and in part supported by the National Yang Ming Chiao Tung University-Kaohsiung Medical University Joint Research Project (#NYCU-KMU-111-I002) from Taiwan.

Appendix A. Supplementary material

Supplementary data associated with this article can be found in the online version at doi:10.1016/j.snb.2023.133960.

References

[1] M. Mitratza, B.M. Goodale, A. Shagadatova, V. Kovacevic, J. van de Wijgert, T. B. Brakenhoff, et al., The performance of wearable sensors in the detection of SARS-CoV-2 infection: a systematic review, Lancet Digit. Health 4 (2022) e370–e383.
[2] E.D. Nascimento, W.T. Fonseca, T.R. de Oliveira, C.R.S.T.B. de Correia, V.M. Faça, B.P. de Morais, et al., COVID-19 diagnosis by SARS-CoV-2 Spike protein detection in saliva using an ultrasensitive magneto-assay based on disposable electrochemical sensor, Sens. Actuator B Chem. 353 (2022), 131128.
[3] J. Rodriguez-Manzano, K. Malpartida-Cardenas, N. Moser, I. Pennisi, M. Cavuto, L. Miglietta, et al., Handheld point-of-care system for rapid detection of SARS-CoV-2 extracted RNA in under 20 min, ACS Cen. Sci. 7 (2021) 307–317.
[4] T.T. Le, J.P. Cramer, R. Chen, S. Mayhew, Evolution of the COVID-19 vaccine development landscape, Nat. Rev. Drug Discov. 19 (2020) 667–668.
[5] E. Mahase, Covid-19: UK approves Pfizer and BioNTech vaccine with rollout due to start next week, BMJ Clin. Res. Ed. 371 (2020) m4714.
[6] S. Adibzadeh, S. Amiri, G.E. Nia, M.R. Taleghani, Z.K. Bijarpas, N. Maserat, et al., Therapeutic approaches and vaccination in fighting COVID-19 infections: a review, Gene Rep. 27 (2022), 101619.
[7] D. Sadighbayan, E. Ghafar-Zadeh, Portable sensing devices for detection of COVID-19: a review, IEEE Sens. J. 21 (2021) 10219–10230.
[8] B. Udugama, P. Kadhiresan, H.N. Kozlowski, A. Malekjahani, M. Osborne, V.Y. C. Li, et al., Diagnosing COVID-19: the disease and tools for detection, ACS Nano 14 (2020) 3822–3835.
[9] E. Cesewski, B.N. Johnson, Electrochemical biosensors for pathogen detection, Biosens. Bioelectron. 159 (2020), 112214.
[10] H. Li, X. Liu, L. Li, X. Mu, R. Genov, A.J. Mason, CMOS electrochemical instrumentation for biosensor microsystems: a review, Sensors 17 (2016).
[11] S.I. Kaya, L. Karadurmus, G. Ozcelikay, N. Karadas Bakirhan, S. Ozkan. Electrochemical Virus Detections With Nanobiosensors, 2020, pp. 303–326.
[12] S. Lv, K. Zhang, L. Zhu, D. Tang, R. Niessner, D. Knopp, H$_2$-based electrochemical biosensor with Pd nanowires@ZIF-67 molecular sieve bilayered sensing interface for immunoassay, Anal. Chem. 91 (2019) 12055–12062.
[13] S. Lv, K. Zhang, Q. Zhou, D. Tang, Plasmonic enhanced photoelectrochemical aptasensor with D-A F8BT/g-C$_3$N$_4$ heterojunction and AuNPs on a 3D-printed device, Sens. Actuators B Chem. 310 (2020), 127874.
[14] S. Lv, K. Zhang, L. Zhu, D. Tang, ZIF-8-assisted NaYF$_4$:Yb,Tm@ZnO converter with exonuclease III-powered DNA walker for near-infrared light responsive biosensor, Anal. Chem. 92 (2020) 1470–1476.
[15] M. Ding, X. Cai, H.-L. Jiang, Improving MOF stability: approaches and applications, Chem. Sci. 10 (2019) 10209–10230.

[16] J.F. Olorunyomi, S.T. Geh, R.A. Caruso, C.M. Doherty, Metal–organic frameworks for chemical sensing devices, Mater. Horiz. 8 (2021) 2387–2419.
[17] S. Yuan, L. Feng, K. Wang, J. Pang, M. Bosch, C. Lollar, et al., Stable metal–organic frameworks: design, synthesis, and applications, Adv. Mater. 30 (2018) 1704303.
[18] S. Lv, Y. Tang, K. Zhang, D. Tang, Wet NH_3-triggered NH_2-MIL-125(Ti) Structural switch for visible fluorescence immunoassay impregnated on paper, Anal. Chem. 90 (2018) 14121–14125.
[19] R. Ren, G. Cai, Z. Yu, Y. Zeng, D. Tang, Metal-polydopamine framework: an innovative signal-generation tag for colorimetric immunoassay, Anal. Chem. 90 (2018) 11099–11105.
[20] A. Amini, S. Kazemi, V. Safarifard, Metal-organic framework-based nanocomposites for sensing applications – a review, Polyhedron 177 (2020), 114260.
[21] H.A. Schulze, B. Hoppe, M. Schäfer, D.P. Warwas, P. Behrens, Electrically conducting nanocomposites of carbon nanotubes and metal-organic frameworks with strong interactions between the two components, ChemNanoMat 5 (2019) 1159–1169.
[22] Z. Peng, Z. Jiang, X. Huang, Y. Li, A novel electrochemical sensor of tryptophan based on silver nanoparticles/metal–organic framework composite modified glassy carbon electrode, RSC Adv. 6 (2016) 13742–13748.
[23] Y. Shu, Y. Yan, J. Chen, Q. Xu, H. Pang, X. Hu, Ni and NiO nanoparticles decorated metal–organic framework nanosheets: facile synthesis and high-performance nonenzymatic glucose detection in human serum, ACS Appl. Mater. Interfaces 9 (2017) 22342–22349.
[24] J.C. Garcia, J. Bareño, J. Yan, G. Chen, A. Hauser, J.R. Croy, et al., Surface structure, morphology, and stability of $Li(Ni_{1/3}Mn_{1/3}Co_{1/3})O_2$ cathode material, J. Phys. Chem. C 121 (2017) 8290–8299.
[25] D. Zhang, H. Yan, Y. Lu, K. Qiu, C. Wang, Y. Zhang, et al., NiCo2O4 nanostructure materials: morphology control and electrochemical energy storage, Dalton Trans. 43 (2014) 15887–15897.
[26] S. Zhang, G. Sun, Y. Li, B. Zhang, Y. Wang, Z. Zhang, Enhanced triethylamine gas sensing performance of the porous Zn_2SnO_4/SnO_2 hierarchical microspheres, J. Alloy. Compd. 785 (2019) 382–390.
[27] T. Zhu, Z.Y. Ang, G.W. Ho, Self-assembly formation of $NiCo_2O_4$ superstructures with porous architectures for electrochemical capacitors, RSC Adv. 5 (2015) 53259–53266.
[28] M. Zukalova, J. Prochazka, B. Pitna Laskova, A. Zukal, L. Kavan, Layered $LiNi_{1/3}Mn_{1/3}Co_{1/3}O_2$ (NMC) with optimized morphology for Li-ion batteries, ECS Trans. 87 (2018) 67.
[29] S.E. Moosavifard, J. Shamsi, M. Ayazpour, 2D high-ordered nanoporous $NiMoO_4$ for high-performance supercapacitors, Ceram. Int. 41 (2015) 1831–1837.
[30] J. Wu, R. Mi, S. Li, P. Guo, J. Mei, H. Liu, et al., Hierarchical three-dimensional NiCo2O4 nanoneedle arrays supported on Ni foam for high-performance supercapacitors, RSC Adv. 5 (2015) 25304–25311.
[31] H.-Q. Xu, K. Wang, M. Ding, D. Feng, H.-L. Jiang, H.-C. Zhou, Seed-mediated synthesis of metal–organic frameworks, J. Am. Chem. Soc. 138 (2016) 5316–5320.
[32] F. Carson, J. Su, A.E. Platero-Prats, W. Wan, Y. Yun, L. Samain, et al., Framework isomerism in vanadium metal–organic frameworks: MIL-88B(V) and MIL-101(V), Cryst. Growth Des. 13 (2013) 5036–5044.
[33] A. Dhakshinamoorthy, M. Alvaro, P. Horcajada, E. Gibson, M. Vishnuvarthan, A. Vimont, et al., Comparison of porous iron trimesates basolite F300 and MIL-100 (Fe) as heterogeneous catalysts for lewis acid and oxidation reactions: roles of structural defects and stability, ACS Catal. 2 (2012) 2060–2065.
[34] S. Ma, D. Sun, M. Ambrogio, J.A. Fillinger, S. Parkin, H.-C. Zhou, Framework-catenation isomerism in metal−organic frameworks and its impact on hydrogen uptake, J. Am. Chem. Soc. 129 (2007) 1858–1859.
[35] J. Hafizovic, M. Bjørgen, U. Olsbye, P.D.C. Dietzel, S. Bordiga, C. Prestipino, et al., The inconsistency in adsorption properties and powder xrd data of MOF-5 is rationalized by framework interpenetration and the presence of organic and inorganic species in the nanocavities, J. Am. Chem. Soc. 129 (2007) 3612–3620.
[36] L. Wang, Y. Zhang, X. Li, Y. Xie, J. He, J. Yu, et al., The MIL-88A-derived Fe_3O_4-carbon hierarchical nanocomposites for electrochemical sensing, Sci. Rep. 5 (2015) 14341.
[37] S. Wang, Y. Liao, O.K. Farha, H. Xing, C.A. Mirkin, Electrostatic purification of mixed-phase metal–organic framework nanoparticles, Chem. Mater. 30 (2018) 4877–4881.
[38] S. Palanisamy, H.-M. Wu, L.-Y. Lee, S.-S.F. Yuan, Y.-M. Wang, Fabrication of 3D amino-functionalized metal–organic framework on porous nickel foam skeleton to combinate follicle stimulating hormone antibody for specific recognition of follicle-stimulating hormone, J. Am. Chem. Soc. Au 1 (2021) 2249–2260.
[39] Y. Li, C. Lin, Y. Peng, J. He, Y. Yang, High-sensitivity and point-of-care detection of SARS-CoV-2 from nasal and throat swabs by magnetic SERS biosensor, Sens. Actuators B Chem. 365 (2022), 131974.
[40] G. Mao, Y. Li, G. Wu, S. Ye, S. Cao, W. Zhao, et al., Construction of ratiometric Si-Mn:ZnSe nanoparticles for the immunoassay of SARS-CoV-2 spike protein, Sens. Actuators B Chem. 369 (2022), 132306.
[41] T. Perkmann, N. Perkmann-Nagele, T. Koller, P. Mucher, A. Radakovics, R. Marculescu, et al., Anti-spike protein assays to determine SARS-CoV-2 antibody levels: a head-to-head comparison of five quantitative assays, Microbiol. Spectr. 9 (2021) e00247–e002421.

Sathyadevi Palanisamy received her M.S. degree in Madurai Kamaraj University in 2007. She completed her M.Phil. degree in Bharathiar University in 2009. She obtained her Ph.D. degree in Bharathiar University in 2012. Currently, she is working as a Post-doctoral fellow under the supervision of Prof. Yun-Ming Wang at Department of Biological Science and Technology, Institute of Molecular Medicine and Bioengineering, National Yang-Ming Chiao Tung University, Taiwan. Her research interests focus on metal-organic frameworks and their applications in biosensors.

Li-Yun Lee is a master student working under Prof. Yun-Ming Wang at Department of Biological Science and Technology, Institute of Molecular Medicine and Bioengineering, National Yang-Ming Chiao Tung University, Taiwan. Her research interests focus on metal-organic frameworks and their applications in biosensors.

Chih-Fei Kao is a Assistant Professor in the Department of Biological Science and Technology, Institute of Molecular Medicine and Bioengineering, National Yang-Ming Chiao Tung University, Taiwan. Research interests include brain aging and neuronal contribution to animal lifespan and temporal behavior of neural stem cells.

Wen-Liang Chen is the Associate Dean in the Department of Biological Science and Technology, Institute of Molecular Medicine and Bioengineering, National Yang-Ming Chiao Tung University, Taiwan. His research expertize includes proteomics, immunochemistry, immunoassay, and antibody engineering.

Hsiang-Ching Wang obtained his Ph.D degree in the Department of Biological Science and Technology, Institute of Molecular Medicine and Bioengineering, National Yang-Ming Chiao Tung University, Taiwan. He is a researcher working in the Biomedical Technology and Device Research Lab, Industrial Technology Research Institute, Hsinchu 300, Taiwan.

San-Tai Shen is working in AnTaimmu BioMed Co., Ltd, located at Hsinchu, Taiwan.

Shyng-Shiou F. Yuan is a Medical Doctor and Professor working in Translational Research Center, Department of Obstetrics and Gynecology, Faculty and College of Medicine at both Kaohsiung Medical University Hospital, Kaohsiung Medical University.

Yu-An Kung is working as a Post-doctoral fellow in the Research Center for Emerging Viral Infections, College of Medicine, Chang Gung University located at Taoyuan, Taiwan.

Yun-Ming Wang is a Professor in Department of Biological Science and Technology, Institute of Molecular Medicine and Bioengineering, National Yang-Ming Chiao Tung University, Taiwan. His current research interests include the probe for optical and molecular imaging, bioinorganic chemistry, metal-organic frameworks, paramagnetic metal complex and bio-activated metal complex for magnetic resonance imaging(MRI), superparamagnetic iron oxide nanoparticle (SPIO) for magnetic resonance imaging (MRI). The focus is extended on the application studies of fluorescent sensors and biosensors.

Jhih-Wei Jian is working in AnTaimmu BioMed Co., Ltd, located at Hsinchu, Taiwan.